


Transmit Beamforming for Underwater Acoustic OFDM Systems

Diego A. Cuji , *Graduate Student Member, IEEE*, and Milica Stojanovic, *Fellow, IEEE*

Abstract—This article addresses the problem of transmit beamforming for underwater acoustic communication systems within the framework of multicarrier signaling based on orthogonal frequency division multiplexing (OFDM). The system consists of a transmitter equipped with a uniform linear array and a single receiver. Transmit beamforming requires the transmitter to have complete knowledge of the channel to the receiver; however, this assumption is often not justified in acoustic channels with long feedback delays. To counteract this problem, we propose a technique that targets only those features of the channel that can withstand the feedback delay. One such feature is the angle of arrival of the principal propagation path, which does not experience rapid variations caused by surface scattering, and is thus, varying sufficiently slowly that it can tolerate long feedback delays. OFDM provides an ideal platform for implementing broadband beamforming, and we study the system performance in terms of the data detection mean squared error (MSE) and bit error rate (BER), using synthetic data transmitted over a 1 km shallow water channel in the 10–15 kHz acoustic band. Specifically, we show that beamforming in the principal path's direction achieves excellent MSE performance, with only a few dB degradation with respect to optimal beamforming. We present results for different receive-side detection methods, namely, differentially coherent detection and coherent detection. In addition, we propose an angle tracking algorithm to reduce the complexity in mobile systems, and we demonstrate the system performance using an over-the-air acoustic communications testbed.

Index Terms—Acoustic feedback, channel estimation, differentially coherent detection, null-steering, orthogonal frequency division multi-plexing (OFDM), path-identification, transmit beamforming, underwater acoustic communications.

I. INTRODUCTION

WE CONSIDER the use of transmit beamforming for underwater acoustic systems with multicarrier modulation based on orthogonal frequency division multiplexing (OFDM) modulation. Our work is motivated by the fact that acoustic OFDM has been demonstrated in practice to be an excellent approach for high speed underwater communications [1], [2], [3]; however, it has not been considered in conjunction with transmit beamforming. Transmit beamforming has meanwhile been

investigated extensively for terrestrial radio applications, both in point-to-point (single user) and in point-to-multipoint (multiuser) scenarios, showing substantial benefits in both cases [4].

Transmit beamforming is based on the notion that multiple transmitter elements apply different weights such that the signals transmitted from the array add constructively at the receiver. In an optimal setting, each transmitter element uses a weight proportional to the complex conjugate of the channel transfer function to the receiver.

The problem that arises when trying to implement the optimal channel-based beamforming in practice is that the assumption of complete channel knowledge may not be sufficiently accurate, as the transmitter acquires the channel state information (CSI) via feedback from the receiver. The transmitter, thus, only has partial knowledge of the channel, as the channel estimate is not only noisy, but can be outdated if the channel has changed during the time it took to close the feedback loop. The difficulties are particularly pronounced in time-varying underwater acoustic channels, as the feedback delay is large as compared to the channel coherence time due to the low speed of sound propagation.

The literature on feedback-based underwater acoustic communications remains scarce despite the general understanding of the feedback benefits [5]. An experimental analysis of a feedback-based acoustic system operating with adaptive OFDM modulation can be found in [6]. Transmit arrays, however, are not considered in this reference. A larger body of work that touches on the topic of acoustic feedback and transmit arrays is that of time-reversal mirrors or phase-conjugate arrays, which have mainly been considered within the framework of single-carrier broadband modulation [7], [8], [9]. In these systems, the transmitter simply time-reverses a reference signal sent by the receiver (or effectively, phase conjugates it in the frequency domain), adequately adjusting its weights in this manner. It is well known, however, that this procedure alone does not suffice to build a system capable of operating over a frequency-selective and time-varying acoustic channel.

Liao et al. [10] proposed a method for informing the transmitter about the CSI based on having a bank of prerecorded channel responses. The receiver is assumed to be located on a spatial grid, and the channels between the transmit array and each grid point are previously known to both the transmitting and receiving sides. The transmitter sends a pilot signal in response to which the receiver estimates the channel and compares it to the precomputed channels. The best match indicates the location of the receiver and its CSI estimate. The receiver then sends

Manuscript received 29 August 2022; revised 18 March 2023; accepted 7 July 2023. Date of publication 13 September 2023; date of current version 8 February 2024. This work was supported by the Office of Naval Research under Grant N00014-20-1-2453. (Corresponding author: Diego A. Cuji.)

Associate Editor: Y. R. Zheng.

Diego A. Cuji is with Electrical Engineering, Northeastern University, Boston, MA 02115 USA (e-mail: cujidan.d@northeastern.edu).

Milica Stojanovic is with Northeastern University, Boston, MA 02115 USA (e-mail: millitsa@ece.neu.edu).

Digital Object Identifier 10.1109/JOE.2023.3295474

back the grid point index so that the transmitter can obtain the precomputed CSI corresponding to the particular grid point. While this procedure eliminates the need for explicit channel estimation at the transmitter end, it does not eliminate the problem of time-variation and the ensuing errors.

The authors in [11] and [12] proposed a transmit beamforming method for use in conjunction with a medium access control (MAC) protocol within a network of underwater vehicles. A separate spatial beam is formed in a probabilistic manner towards each vehicle whose location can be resolved from that of other vehicles. The beam width and direction are kept within a certain range to account for motion-induced localization uncertainty, which is modeled as Gaussian.

The aim of the present work is to address the problem of transmit beamforming over a time-varying acoustic channel within the OFDM system framework. Specifically, we address the question of whether a feature of the channel exists that is varying slowly enough that it can withstand the feedback delay, and can be exploited in an efficient manner.

The time-varying behavior of the acoustic channel is mainly caused by unstable signal propagation paths, whose gains and delays are governed by small-scale fading, and cannot be predicted with sufficient accuracy. This fact suggests exploration of the paths' angles of arrival. This would lead to the design of a suboptimal transmit beamforming strategy that might still provide benefits as long as the propagation paths can be resolved in space. Even though the paths' angles might vary over the feedback delay, the change may be small enough to justify such an approach. Therefore, we introduce a transmit beamforming strategy based on the direction of the stable principal path. The stable principal path can be the line-of-sight or any other path that does not experience rapid small-scale fading.

The direction of arrival estimation has been widely studied for several decades [13], [14], [15]. Here, we propose a method for estimating the principal path's angle of arrival from the post-fast Fourier transform (FFT) OFDM signals, taking into account the broadband nature of acoustic communication signals. We label this strategy as angle-based beamforming to distinguish it from the channel-based beamforming, which uses an estimate of the full channel response to construct the beamforming weights.

The transmit beamforming techniques are demonstrated on a simulated 1 km shallow water channel in the 10–15 kHz acoustic band. As a proof of concept, we also demonstrate the system performance using over-the-air acoustic transmissions, which enable the use of the acoustic feedback in real time in a controlled experimental setup. The proposed methods achieve excellent performance, demonstrating the capability to withstand the acoustic feedback delay in the over-the-air environment.

The rest of this article is organized as follows. In Section II, we introduce the system and channel model. Section III discusses the transmit beamforming techniques, specifically channel-based and angle-based beamforming methods. Section IV contains the simulation results. In Section V, we study the array aperture size and interelement spacing selection, and Section VI introduces angle tracking. Section VII presents the experimental results. Finally, Section VIII concludes this article.

II. SYSTEM AND CHANNEL MODEL

We consider an OFDM communication system with M_t transmit array elements, a single receiver element, and K carriers within a total bandwidth B . We assume a vertical array with interelement spacing d , and a system geometry that justifies the assumption of plane wave propagation. The receiver is positioned at a horizontal distance L_{TR} and an elevation angle θ_0 with respect to the transmitter, as illustrated in Fig. 1.

At the onset of communication, the receiver sends a probe signal to the transmitter. In response, the transmitter adjusts its beamforming weights, forms an information signal, and sends it back to the receiver. The receiver can implement differentially coherent detection or coherent detection.

A. Channel Model

The channel is frequency selective due to multipath propagation, and it is also time-varying. In a properly designed OFDM system, time-variation is negligible over the duration of one OFDM block (there is no intercarrier interference); however, the channel might change over the feedback time, during which the receiver–transmitter positioning might vary slightly. As a result, the channel measured on the uplink (receiver to transmitter) may differ from the channel measured on the downlink (transmitter to receiver), since the time it takes to close the feedback loop is at least $2L_{TR}/c$, where c is the speed of sound in water (nominally 1500 m/s).

At time t , the channel transfer function between two points is modeled as [16]

$$H(f, t) = \sum_{p=0}^{P-1} h_p \gamma_p(f, t) e^{-j2\pi f \tau_p(t)} \quad (1)$$

where the coefficients h_p represent the path amplitudes, $\gamma_p(f, t)$ are the small-scale fading coefficients, $\tau_p(t) = \tau_p - a_p(t)$ are the path delays, and P is the number of propagation paths. The factor $a_p(t)$ is the Doppler scaling factor, which models the residual motion-induced frequency shifting after front-end frequency offset compensation. In other words, $a_p(t)$ is assumed to be small, e.g., on the order of 10^{-5} , and in general invariant over the duration of one OFDM block. With proper processing, it can also be removed (more details can be found in [2]). The path $p = 0$ represents the principal and stable path, which in shallow water may be the direct path with no surface-bottom reflections.

Focusing on post-FFT processing, we are interested in the equivalent channel response evaluated at carrier frequencies $f_k = f_0 + k\Delta f$, $k = 0, \dots, K-1$, where f_0 is the first carrier frequency, and $\Delta f = 1/T$ is the carrier separation (inverse of the OFDM block duration T). During the uplink transmission, the equivalent channel pertaining to the m th element and the k th carrier is denoted by $H_k^{m,\text{up}} = \sum_p h_p^{m,\text{up}} \gamma_{p,k}^{m,\text{up}} e^{-j2\pi f_k \tau_p^{m,\text{up}}}$. Similarly, during the subsequent downlink transmission, the equivalent channels are denoted by $H_k^{m,\text{dn}} = \sum_p h_p^{m,\text{dn}} \gamma_{p,k}^{m,\text{dn}} e^{-j2\pi f_k \tau_p^{m,\text{dn}}}$. The relevant channel parameters (path gains, small-scale coefficients and

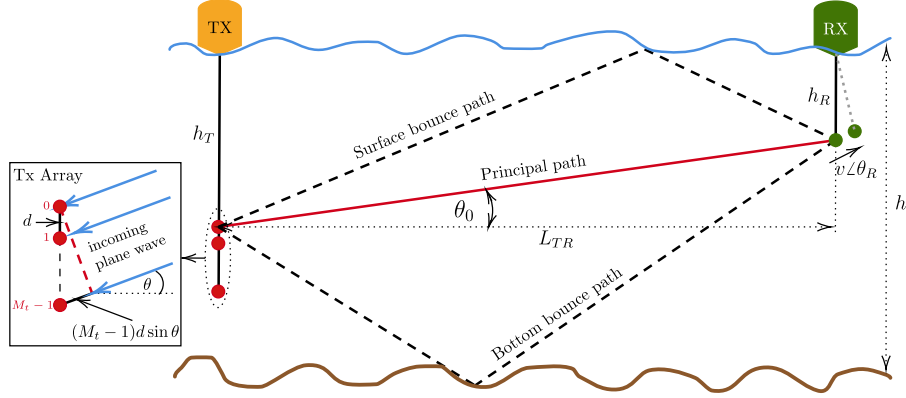


Fig. 1. System geometry of a shallow water channel.

delays) pertain to the transmitter–receiver positioning at the times of uplink and downlink transmissions.

Assuming that the uplink–downlink cycle takes a few seconds, drifting will cause only a small change in positioning, e.g., on the order of a meter. The corresponding change in the path gains is likely to be negligible for a typical link spanning a range on the order of a kilometer; however, the change in path delays and the small-scale fading coefficients could cause the overall channel response to change significantly. If there is absolutely no transmitter–receiver motion, surface motion will still cause a change in the delays of those paths that encounter it, while surface scattering will induce micromultipath and dispersion. Time and frequency correlation of a small-scale fading coefficient $\gamma_p(f, t)$ are described through the Doppler bandwidth of the random micropath delay deviations [16]. Spatial correlation between the small-scale fading coefficients corresponding to the same path but different array elements is meanwhile governed by the element spacing. So long as the surface encounter points corresponding to the same path and different array elements are separated by more than a few wavelengths, their small-scale fading coefficients can be regarded as uncorrelated. As an example, let us look at a system operating in the 10–15 kHz bandwidth (maximum wavelength 0.15 m) over a distance $L_{TR} = 1500$ m, with transmitter and receiver suspended at a depth of 75 m, and interelement spacing $d = 0.3$ m. Considering the path with a single surface reflection, reflection points corresponding to adjacent array elements are spaced by 3 m, which well exceeds the maximum wavelength. Hence, their small-scale fading coefficients can be regarded as uncorrelated. From the viewpoint of beamforming, such a path is not stable.

III. BEAMFORMING

In systems whose bandwidth is much smaller than the center frequency, beamforming is typically considered in the narrowband context, i.e., the beamforming weights are the same for all signal frequencies. In acoustic systems, however, the narrowband assumption may not be justified, as the bandwidth $B = K\Delta f$ may not be negligible compared to the carrier frequencies f_k . In that case, it is advantageous to consider

broadband beamforming, where the beamformer coefficients are evaluated separately for each carrier frequency.

Let us denote by $\mathbf{w}_k = [w_k^0 \ w_k^1 \ \dots \ w_k^{M_t-1}]^\top$ the vector of beamformer coefficients corresponding to carrier k . The OFDM signal transmitted on the downlink from the m th array element is then given by¹

$$s_m^{\text{dn}}(t) = \text{Re} \left\{ \sum_{k=0}^{K-1} d_k^{\text{dn}} w_k^{m*} e^{j2\pi f_k t} \right\}, \quad t \in [-T_g, T] \quad (2)$$

where $m = 0, \dots, M_t - 1$, d_k^{dn} is the information data symbol belonging to a unit-amplitude phase-shift keying (PSK) alphabet for either differentially coherent detection or quadrature-amplitude modulation (QAM) for coherent detection, and T_g is the length of the guard interval (cyclic prefix) between the OFDM blocks.

The signal received on the k th carrier after front-end synchronization and FFT demodulation is given by

$$\begin{aligned} y_k^{\text{dn}} &= d_k^{\text{dn}} \sum_{m=0}^{M_t-1} w_k^{m*} H_k^{m,\text{dn}} + z_k^{\text{dn}} \\ &= d_k^{\text{dn}} \mathbf{w}_k' \mathbf{H}_k^{\text{dn}} + z_k^{\text{dn}} \\ &= d_k^{\text{dn}} H_k^{\text{eq}} + z_k^{\text{dn}} \end{aligned} \quad (3)$$

where z_k^{dn} is the zero-mean downlink noise with variance σ_{dn}^2 , $\mathbf{H}_k^{\text{dn}} = [H_k^{0,\text{dn}} \ H_k^{1,\text{dn}} \ \dots \ H_k^{M_t-1,\text{dn}}]^\top$ is the downlink channel vector, and H_k^{eq} is the equivalent downlink channel coefficient corresponding to the k th carrier.

The OFDM signal transmitted on the uplink is given by

$$s^{\text{up}}(t) = \text{Re} \left\{ \sum_{k=0}^{K-1} d_k^{\text{up}} e^{j2\pi f_k t} \right\}, \quad t \in [-T_g, T]. \quad (4)$$

For purposes of transmit-side adaptation, some or all of the data symbols d_k^{up} are regarded as pilots, i.e., they are set to a priori known values, e.g., 1. After time synchronization, initial resampling, frequency offset compensation, and FFT demodulation,

¹Complex conjugate and conjugate transpose are denoted by $(\cdot)^*$ and $(\cdot)'$, respectively.

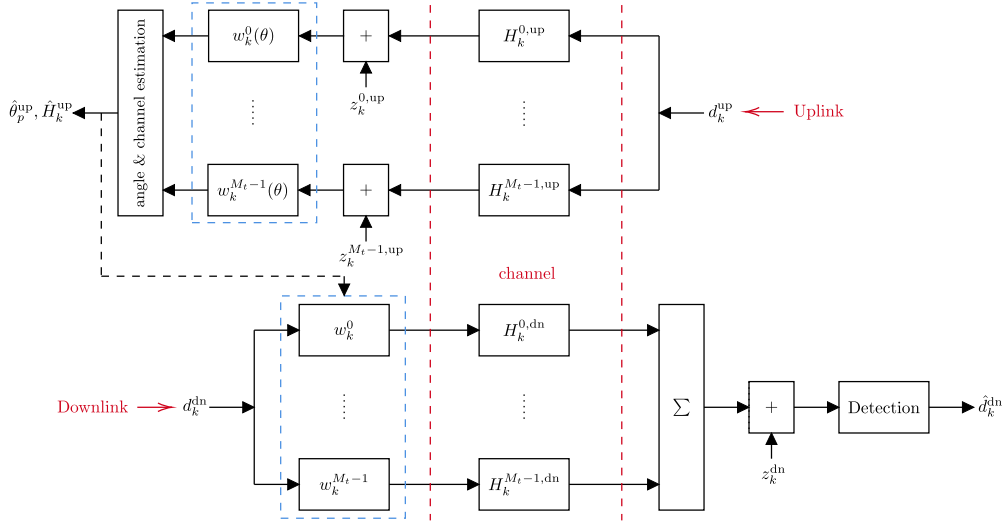


Fig. 2. Uplink transmission (above) and downlink transmission (below).

the uplink pilot signal received across the array on carrier k is modeled as

$$\mathbf{x}_k^{up} = \mathbf{H}_k^{up} + \mathbf{z}_k^{up} \quad (5)$$

where \mathbf{z}_k^{up} is the uplink noise, assumed to be zero-mean with covariance $\sigma_{up}^2 \mathbf{I}_{M_t}$, where \mathbf{I}_{M_t} is a $M_t \times M_t$ identity matrix and $\mathbf{H}_k^{up} = [H_k^{0,up} \ H_k^{1,up} \ \dots \ H_k^{M_t-1,up}]^T$ is the uplink channel vector. These signals are used to adjust the beamformer weights. Fig. 2 summarizes the uplink and the downlink system functions.

A. Optimal Beamforming

The beamformer weights that maximize the signal-to-noise ratio (SNR) in the received signal (3) are given by $\mathbf{w}_k = C_k^{dn} \mathbf{H}_k^{dn}$, $k = 0, \dots, K-1$, where C_k^{dn} are arbitrary constants [4], [17]. These constants are chosen such that $(1/K) \sum_k \mathbf{w}_k' \mathbf{w}_k = 1$, thus, ensuring that no additional power is expanded through the process of beamforming.

However, perfect knowledge of the downlink channel may not be available at the transmit side since: 1) the channel is time-varying; and 2) channel estimation is performed in the presence of noise. In what follows, we study two ways of determining the beamformer coefficients: 1) beamforming with delayed and noisy channel information; and 2) beamforming in the principal path's direction. As a comparison benchmark, we will also consider the case in which no beamformer adjustment is made, i.e., $w_k^m = 1/\sqrt{M_t}$.

B. Beamforming With Delayed and Noisy Channel Information

In this case, the beamformer weights are formed using an estimate of the downlink channel $\hat{\mathbf{H}}_k^{dn}$ instead of the true value \mathbf{H}_k^{dn} , for $k = 0, \dots, K-1$. The estimate is obtained from the uplink pilot signals (5). Various approaches to channel estimation are possible, but we will not concentrate our analysis on algorithm details. Instead, we will utilize several benchmark cases. The first case is that of a noiseless estimate, $\hat{\mathbf{H}}_k^{dn} = \mathbf{H}_k^{up}$,

in this scenario, the channel information is simply delayed. Any practical estimation method will perform worse than this benchmark. An improvement to this case can be sought only through prediction. Prediction in turn relies on the knowledge of the statistical channel model that governs the behavior of the random coefficients $\gamma_p^m(f, t)$. Acquisition of such a model is not a simple task, and is itself likely to result in estimation errors when carried out in the presence of noise.

The second case is that of simple time-reversal, where $\hat{\mathbf{H}}_k^{dn} = \mathbf{H}_k^{up} + \mathbf{z}_k^{up}$, and the noise components are characterized by the variance σ_{up}^2 . A practical channel estimation method operates in the impulse response domain to optimally exploit the frequency correlation by capitalizing on the fact that the channel is sparse, i.e., that only $L_{up} < K$ taps suffice to represent it. An example of such a method is least squares (LS) estimation that extracts $L_{up} = \lceil BT_{mp} \rceil$ taps, where T_{mp} is the multipath spread of the channel. In this case, a noisy estimate is obtained as $\hat{\mathbf{H}}_k^{dn} = \mathbf{H}_k^{up} + \tilde{\mathbf{z}}_k^{up}$, where the variance of the noise components is reduced to $\tilde{\sigma}_{up}^2 = (L_{up}/K)\sigma_{up}^2$.

C. Beamforming in the Principal Path's Direction

When feedback delay is long such that it leads to too much discrepancy between the true and the estimated channel response, one must seek some feature of the channel that can still be exploited, and that feature may be the principal path's angle of arrival. Given a vertical array and a typical channel where the transmission distance L_{TR} is much greater than the communication channel depth, propagation delays across the array elements are related as follows:

$$\tau_p^m = \tau_p^0 + m \frac{d}{c} \sin \theta_p, \quad m = 0, \dots, M_t - 1 \quad (6)$$

where θ_p is the p th path's angle of arrival, $p = 0, \dots, P-1$. Note that a proper time synchronization in reference to the first element implies $\tau_0^0 = 0$. The underlying assumption is that d is small enough such that all the array elements see the same angle of arrival.

We are interested in the stable, principal path that arrives at an angle θ_0 . Beamforming to the principal path is a plausible approach under the assumption that the angle θ_0 changes little over the time needed to close the feedback loop. This assumption is well justified for many cases. Consider a 1.5 km link where the round-trip propagation time is 2 s. Drifting at 1 m/s will cause the receiver to move by 2 m. Even if the motion is in the direction that changes the angle the most, compounded onto 1.5 km, a 2 m displacement will not affect the angle of arrival in any significant way. This fact is key to our treatment, and we conjecture that the angle of arrival is that parameter which does not change much over the feedback time, i.e., we assume that $\theta_0^{\text{up}} = \theta_0^{\text{dn}} = \theta_0$, and exploit this feature of the channel to design the beamformer. In general, the beamforming weights pointing in the direction θ are given by

$$w_k^m(\theta) = \frac{1}{\sqrt{M_t}} e^{-j2\pi m f_k \frac{d}{c} \sin \theta}, \quad m = 0, \dots, M_t - 1, \\ k = 0, \dots, K - 1. \quad (7)$$

In our case, we wish to point the beam in the direction θ_0 of the principal path; however, the angle θ_0 is not known and must be estimated.

1) *Estimating the Principal Path's Angle of Arrival:* Estimation of θ_0 can be performed by hypothesizing an angle θ , and defining the vector

$$\mathbf{w}_k(\theta) = [w_k^0(\theta) \ w_k^1(\theta) \ \dots \ w_k^{M_t-1}(\theta)]^\top.$$

Beamforming on the k th carrier of the uplink signal now yields an output $\mathbf{w}_k'(\theta) \mathbf{x}_k^{\text{up}}$, whose total power is

$$S(\theta) = \sum_{k=0}^{K-1} |\mathbf{w}_k'(\theta) \mathbf{x}_k^{\text{up}}|^2. \quad (8)$$

The principal path's angle of arrival is estimated as that angle which maximizes the total power

$$\hat{\theta}_0 = \arg \max_{\theta} S(\theta). \quad (9)$$

The angle $\hat{\theta}_0$ is finally used to construct the beamforming vector $\mathbf{w}_k = \mathbf{w}_k(\hat{\theta}_0)$. This approach is referred to as broadband angle-based beamforming.

The narrowband counterpart employs the same beamforming vector on all the carriers, i.e., $\mathbf{w}_k = \mathbf{w}_0(\hat{\theta}_0)$, the vector corresponding to the lowest carrier frequency f_0 . Center frequency could be used as well, or for that matter, any frequency within the signal bandwidth because the main assumption for this type of beamforming is that the system is narrowband, i.e., that $B \ll f_k, \forall k$. In numerical evaluation, we will include narrowband beamforming as a benchmark, to quantify the advantage of using broadband beamforming over acoustic channels.

D. Broadband Null-Steering

In addition to beamforming in the principal path direction, the transmit array can implement null-steering to place spatial nulls in directions that are undesired, such as the directions of the paths with lower energy. The null-steering algorithm finds a vector $\tilde{\mathbf{w}}_k(\theta_0)$ which:

- 1) maximizes the inner product magnitude $|\tilde{\mathbf{w}}_k'(\theta_0) \mathbf{w}_k(\theta_0)|$, where $\mathbf{w}_k(\theta_0)$ is a steering vector pointing in the desired direction θ_0 ;
- 2) maintains the energy constraint $\|\tilde{\mathbf{w}}_k(\theta_0)\| = 1$;
- 3) places spatial nulls in the undesired directions, $\tilde{\mathbf{w}}_k'(\theta_0) \mathbf{w}_k(\theta_p) = 0$ for $\forall p \neq 0$.

Let us form the matrix \mathbf{W}_k , whose columns are the beamforming vectors $\mathbf{w}_k(\theta_p)$ for $\forall p \neq 0$. The optimal solution $\tilde{\mathbf{w}}_k(\theta_0)$ lies in the subspace that is orthogonal to the one spanned by the columns of \mathbf{W}_k . Thus, maximizing $|\tilde{\mathbf{w}}_k'(\theta_0) \mathbf{w}_k(\theta_0)|$ is equivalent to maximizing $|\tilde{\mathbf{w}}_k'(\theta_0) \mathbf{P}_k \mathbf{w}_k(\theta_0)|$, where \mathbf{P}_k is the orthogonal projection matrix, which is expressed as [18]

$$\mathbf{P}_k = \mathbf{I}_{M_t} - \mathbf{W}_k (\mathbf{W}_k' \mathbf{W}_k)^{-1} \mathbf{W}_k'. \quad (10)$$

Maximization of $|\tilde{\mathbf{w}}_k'(\theta_0) \mathbf{P}_k \mathbf{w}_k(\theta_0)|$ is performed by evoking the Cauchy-Schwartz inequality, yielding

$$\tilde{\mathbf{w}}_k(\theta_0) = \alpha_k \mathbf{P}_k \mathbf{w}_k(\theta_0) \quad (11)$$

where α_k is a constant that is chosen such that $\|\tilde{\mathbf{w}}_k(\theta_0)\| = 1$.

E. Data Detection

The aim of any communication system is to accurately decode the data symbols transmitted through the channel. The received baseband signal (3) shows the dependence on the inner product between the beamformer vector \mathbf{w}_k and the downlink channel vector \mathbf{H}_k^{dn} , which for the case of optimal beamforming can be expressed as $y_k^{\text{dn}} = d_k^{\text{dn}} H_k^{\text{eq}} + z_k^{\text{dn}}$, where $H_k^{\text{eq}} = C_k^{\text{dn}} |\mathbf{H}_k^{\text{dn}}|^2$ is a positive constant, and as such does not influence PSK data detection. Practical (suboptimal) beamforming techniques require additional processing to compensate for residual distortions caused by the equivalent channel $H_k^{\text{eq}} = \mathbf{w}_k' \mathbf{H}_k^{\text{dn}}$.

If coherent detection is used, the coefficients H_k^{eq} are estimated using pilot carriers, e.g., via conventional least squares (LS) techniques, or by applying the path-identification (PI) algorithm [3], which finds the individual channel path gains and delays. Once the channel estimate is available, the estimate of the data symbol is expressed as

$$\hat{d}_k^{\text{dn}} = \frac{y_k^{\text{dn}} \hat{H}_k^{\text{eq}*}}{|\hat{H}_k^{\text{eq}}|^2} \quad (12)$$

where \hat{H}_k^{eq} is the estimate of the channel coefficient on the k th carrier.

Differentially coherent detection is a simpler detection technique that takes advantage of the channel correlation in the frequency domain [1] and eliminates the need for channel estimation. The original PSK data symbols b_k^{dn} are differentially encoded across the carriers to form the transmitted data symbols $d_k^{\text{dn}} = b_k^{\text{dn}} d_{k-1}^{\text{dn}}$ (the encoding process begins with a known symbol $d_0^{\text{dn}} = 1$), and the estimate of the received data symbol is given by

$$\hat{b}_k^{\text{dn}} = \frac{y_{k-1}^{\text{dn}*} y_k^{\text{dn}}}{|y_{k-1}^{\text{dn}}|^2}, \quad k = 1, \dots, K - 1. \quad (13)$$

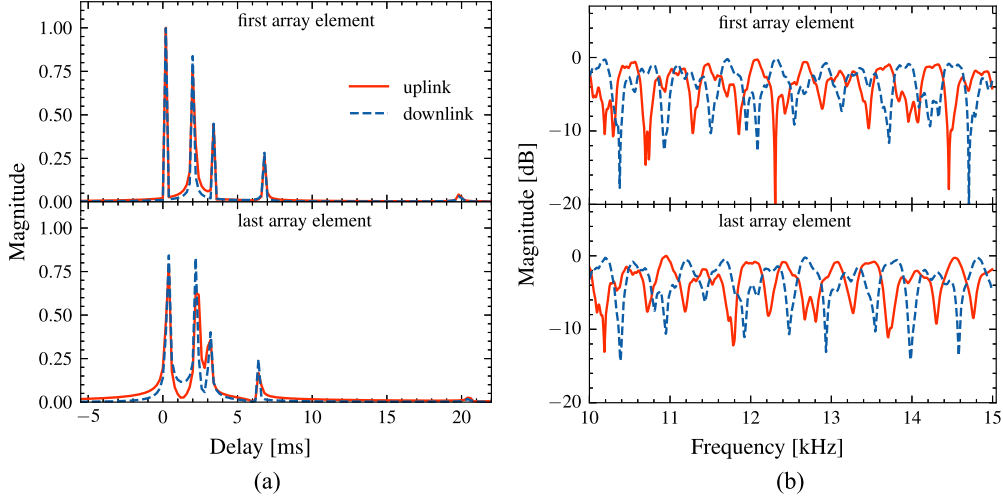


Fig. 3. (a) Impulse responses of the channel as seen on the uplink and downlink. (b) Channel transfer functions on the uplink and downlink.

IV. NUMERICAL RESULTS

In this section, we use an illustrative example to compare the performance of various techniques discussed: optimal beamforming, beamforming with delayed and noisy channel information, and beamforming in the principal path's direction. Performance is evaluated through numerical computation of the mean squared error (MSE) of the detected data symbol and bit error rate (BER) versus SNR.

We focus on an example of a shallow water channel. The channel geometry (see Fig. 1) at the time of uplink transmission is specified by a distance $L_{TR} = 1$ km, receiver depth $h_R = 20$ m, and transmitter depth (top element) $h_T = 70$ m. At the time of downlink reception, we assume that the receiver has drifted at the speed $v = 0.5$ m/s in the direction $\theta_R = 45^\circ$, such that the distance is now $L_{TR} + (2d/c)v \cos \theta_R$, i.e., it has increased by 0.47 m, and the receiver depth is $h_R - (2d/c)v \sin \theta_R$, i.e., it has decreased by 0.47 m. The element spacing is $d = 0.345$ m, and the number of array elements is $M_t = 12$. The speed of sound is taken to be $c = 1500$ m/s in water, and 1300 m/s in the bottom; spherical spreading is assumed for each path. The lowest carrier frequency is $f_0 = 10$ kHz, the bandwidth is $B = 5$ kHz, and the number of carriers is $K = 1024$. The uplink and downlink channels are normalized such that

$$1/(KM_t) \sum_k \sum_m |H_k^{m,\text{up}}|^2 = (1/(KM_t)) \sum_k \sum_m |H_k^{m,\text{dn}}|^2 = 1$$

and the noise variance is taken to be the same on the uplink and downlink, $\sigma_{\text{up}}^2 = \sigma_{\text{dn}}^2 = \sigma^2$. The signal-to-noise ratio is defined as $\text{SNR} = 1/\sigma^2$. Small-scale fading coefficients are generated according to [16] with the following parameters: standard deviation of the surface height displacement is $\sigma_s = c/(5f_0)$, standard deviation of the bottom height displacement is $\sigma_b = c/(3f_0)$, number of micropaths within one path is $S_p = 20$, mean and variance parameters of micropath amplitudes are $\mu_{p,0} = 0$, $\mu_p = 1/S_p$, and $\nu_p = \mu_p/10$, respectively. We demonstrate the performance of the system using three linear modulation

schemes, namely quaternary phase-shift keying (QPSK), 8-PSK, and 16-QAM.

The channel impulse responses on the uplink and downlink, as seen within the system bandwidth, are shown in Fig. 3(a). This channel has $P = 5$ significant paths and the total multipath spread is approximately 20 ms. The gains and delays are calculated from the channel geometry. The channel frequency responses are depicted in Fig. 3(b). Frequency selectivity is pronounced, and the difference between the uplink and the downlink is quite noticeable.

A. Beamforming: Performance Analysis

We consider channel-based beamforming and angle-based beamforming, with and without perfect channel knowledge, in both broadband and narrowband contexts. Channel-based beamforming includes several cases corresponding to the type of channel estimate available at the transmitter: perfect, delayed, time-reversal, and impulse response. Angle-based beamforming cases include perfect beamforming, beamforming with an estimated angle of the principal path, and their narrowband counterparts. A detailed description of these beamforming techniques is given as follows.

- 1) *Perfect*: This case refers to the optimal beamforming method with perfect downlink channel knowledge. The beamforming coefficients are $w_k^m = C_k^{\text{dn}} H_k^{m,\text{dn}2}$.
- 2) *Delayed*: This case corresponds to using a delayed and noiseless channel estimate. The beamformer coefficients are $w_k^m = C_k^{\text{up}} H_k^{m,\text{up}}$.
- 3) *Time-reversal (TR)*: Delayed and noisy channel estimate is used to form the beamformer coefficients as $w_k^m = C_k^{\text{tr}} (H_k^{m,\text{up}} + z_k^{m,\text{up}})$, where the noise variance is σ_{up}^2 .
- 4) *Impulse response (IR)*: In this case, the channel is estimated in the IR domain, e.g., using LS covering L_{up}

²The factors C_k^{dn} , C_k^{up} , C_k^{tr} , and C_k^{ir} are the normalization constants for each of the channel-based beamforming cases, set to ensure that no additional power is expanded through the process of beamforming.

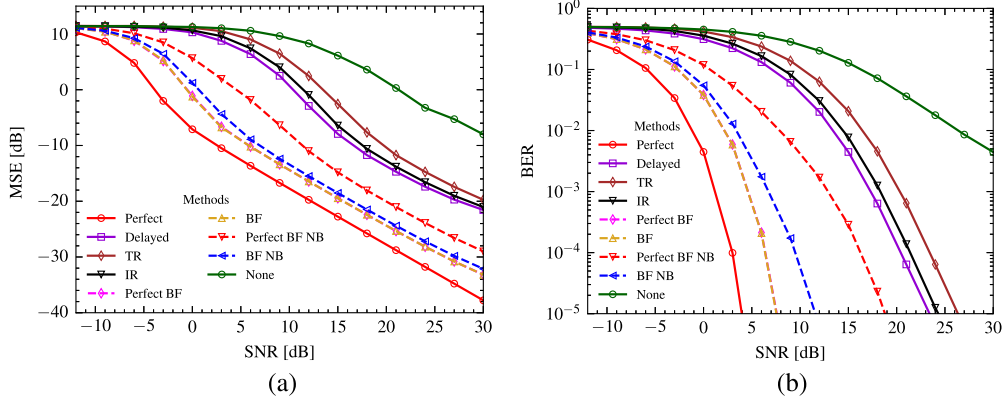


Fig. 4. Performance of various beamforming techniques: average data detection mean squared error (MSE) (a); and bit error rate (BER) (b) as functions of the input SNR. Differentially coherent QPSK detection is used at the receiver.

channel taps spaced by T/K . The beamformer coefficients are $w_k^m = C_k^{\text{tr}}(H_k^{m,\text{up}} + z_k^{m,\text{up}})$, and the noise variance is $(L_{\text{up}}/K)\sigma_{\text{up}}^2$.

- 5) *Perfect beamforming (perfect BF)*: Beamforming in the principal path's direction, $w_k^m = w_k^m(\theta_0)$, with perfect knowledge of θ_0 .
- 6) *Beamforming (BF)*: The principal path's angle of arrival is estimated according to (9), and the beamformer weights are $w_k^m = w_k^m(\hat{\theta}_0)$.
- 7) *Perfect beamforming, narrowband (perfect BF NB)*: The beamformer weights are computed as $w_k^m = w_0^m(\theta_0)$.
- 8) *Beamforming, narrowband (BF NB)*: The beamforming weights are $w_k^m = w_0^m(\hat{\theta}_0)$, where

$$\hat{\theta}_0 = \arg \max_{\theta} \sum_k |\mathbf{w}'_0(\theta) \mathbf{x}_k^{\text{up}}|^2.$$

- 9) *None*: The beamforming coefficients are $w_k^m = 1/\sqrt{M_t}$.

Fig. 4 summarizes performance results in terms of data detection MSE and BER as functions of the input SNR ranging from -10 to 30 dB for $M_t = 12$ transmitter elements. Differentially coherent QPSK detection is implemented at the receiving side, and the data detection MSE is computed as

$$\text{MSE} = \frac{1}{N_r} \frac{1}{K-1} \sum_{i=1}^{N_r} \sum_{k=1}^{K-1} |b_k^{\text{dn}}(i) - \hat{b}_k^{\text{dn}}(i)|^2 \quad (14)$$

where $\hat{b}_k^{\text{dn}}(i)$ is the estimate of the k th data symbol $b_k^{\text{dn}}(i)$ in the i th block. Each OFDM block contains an independent channel and noise realization, and $N_r = 100\,000$ is the total number of realizations.

As one could expect, the performance of all the methods is bounded by that of optimal beamforming (case 1), which provides the lowest MSE in data detection. In contrast to this situation is the case in which no adjustment is made to the beamformer weights (case 9), which yields the highest MSE. The performance of all the other methods lies between these two bounds [see Fig. 4(a)].

Using the delayed channel estimate (case 2) instead of the true channel leads to a substantial performance degradation of about

17 dB. At lower values of the SNR, this degradation implies an MSE high enough to cause a complete system failure (MSE above 0 dB). Simple time-reversal (case 3) exhibits additional degradation, while a more sophisticated channel estimation in the IR domain (case 4) follows the noiseless delayed estimate case closely for the range of SNRs shown. Judging by these results, we conclude that small-scale fading prevents the use of beamforming methods based on transmit-side channel estimation. These observations point to an abrupt contrast between radio channels for which channel-based beamforming is used [4], and acoustic channels where feedback delay clearly presents an obstacle.

Unlike channel-based beamforming, beamforming in the principal path's direction offers a solution to this problem. With perfect channel knowledge, angle-based beamforming (case 5) exhibits only about 3.5 dB degradation of MSE with respect to optimal beamforming (case 1). Most importantly, when working with an estimate of the arrival angle obtained from the noisy uplink data (case 6) instead of the true one, the difference in performance is imperceptible (dashed curves marked with \diamond and \triangle practically coincide). This is a remarkable feature that speaks strongly in favor of practical applicability of feedback-based transmit beamforming for acoustic communications, which has not been fully explored in the past [5].

The performance of narrowband beamforming reveals interesting observations. As expected, ideal narrowband beamforming (case 7) performs worse than ideal broadband beamforming (case 5), losing about 4 dB of MSE. With perfect channel knowledge, angle-based beamforming (case 7) performs about 5 dB (at lower SNR) to 8 dB (at higher SNR) better than channel-based beamforming (case 2). Without perfect channel knowledge, angle-based beamforming (case 8) effectively removes some of the narrowband constraints, as it gains freedom in using an angle that best suits the power metric evaluated over all the signal frequencies—not the angle dictated by a single signal frequency. By doing so, it outperforms the perfect angle-based narrowband beamforming, yielding a performance very close to that of the broadband angle-based beamformer (cases 5 and 6).

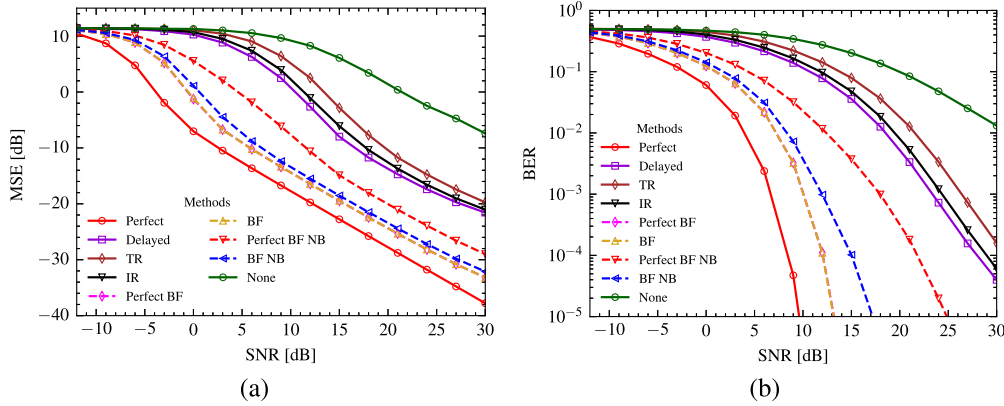


Fig. 5. Performance of various beamforming techniques: average data detection MSE (a) and BER (b) as functions of the input SNR. Differentially coherent 8-PSK detection is used at the receiver.

Fig. 4(b) depicts the performance for various beamforming methods. Optimal channel-based beamforming (case 1) delivers the lowest BER, as opposed to case 9, which leads to the highest BER performance. Without channel knowledge, channel-based methods (cases 2, 3, and 4) need approximately 18, 19, and 22 dB of extra SNR in comparison to case 1 to preserve a 10^{-4} BER. In general, angle-based beamformers outperform channel-based beamformers (cases 2, 3, and 4). We observe that broadband beamforming methods (cases 5 and 6) require only about 3.5 dB of additional SNR to achieve the same BER performance delivered by optimal beamforming with perfect channel knowledge (case 1). Narrowband beamforming with perfect knowledge of θ_0 requires about 10 dB of additional SNR compared to cases 5 and 6 to maintain a 10^{-4} BER. Conversely, narrowband beamforming without perfect knowledge of θ_0 (case 8) requires only about 3 dB of extra SNR to attain the same BER. Narrowband beamforming (case 8) offers a lower computational complexity approach, yielding a somewhat poorer BER performance compared to that of broadband beamforming (case 6). The computational requirements of these methods differ in the computation of $S(\theta)$, which is performed for a range of hypothesized angles $\theta \in [\theta_{\min}, \theta_{\max}]$. For each hypothesized angle in this range (say that there are N_θ such angles), the BF method requires computation of K beamforming vectors $\mathbf{w}_k(\theta)$ for $k = 0, \dots, K-1$. Hence, a total of KN_θ vectors of size $M_t \times 1$ have to be computed. In contrast, the BF NB technique requires only a single vector $\mathbf{w}_0(\theta)$ to be computed for each hypothesized value of θ .

Another possible angle-based beamforming technique consists of computing the beamforming weights for subsets of carrier frequencies instead of for all the carriers. Indeed, computing the weights for fewer carriers provides a reduction in computational complexity, while its performance falls between that of BF and BF NB.

Similarly, Fig. 5 shows the performance results in terms of data detection MSE and BER as functions of the input SNR for $M_t = 12$ transmitter elements for differentially coherent detection using 8-PSK modulation. In this case, the system performance trends of either channel-based beamforming or angle-based beamforming match those observed in Fig. 4 for differentially coherent QPSK detection. We observe that to

achieve the same BER, say 10^{-4} , 8-PSK requires about 5 dB more of the SNR as compared to differential QPSK in all the cases considered.

Coherent detection results based on LS channel estimation are shown in Figs. 6 and 7. In Fig. 6(a) and (b), we illustrate the performance results for QPSK modulation in terms of average MSE and BER, while Fig. 7(a) and (b) contain the 8-PSK and 16-QAM results, respectively. The LS channel estimation targets $L_{\text{dn}} = 80$ taps using $K_{\text{pil}} = 128$ equally spaced pilots in all the cases considered. The data detection MSE is computed as

$$\text{MSE} = \frac{1}{N_r} \frac{1}{K - K_{\text{pil}}} \sum_{i=1}^{N_r} \sum_{k \notin \mathcal{K}_{\text{pil}}} |d_k^{\text{dn}}(i) - \hat{d}_k^{\text{dn}}(i)|^2 \quad (15)$$

where \mathcal{K}_{pil} is the set of K_{pil} pilot carriers, and $\hat{d}_k^{\text{dn}}(i)$ is the estimate of the k th data symbol $d_k^{\text{dn}}(i)$ in the i th block. We see that broadband beamforming (case 6) requires approximately 6 dB of SNR to maintain a 10^{-4} BER using QPSK modulation [see Fig. 6(b)], while it requires approximately 11 dB and 15 dB to maintain the same error rate using 8-PSK [see Fig. 7(a)] and 16 QAM [see Fig. 7(b)] modulation schemes, respectively.

Coherent detection results based on path-identification (PI) algorithm [3] for receive-side channel estimation are illustrated in Fig. 8 for QPSK. The parameters of the path-identification (PI) channel estimation algorithm are the number of paths N_p and the resolution factor I . Particularly, Fig. 8(a) and (b) depict the average MSE and BER, respectively, for total number of paths $N_p = 80$ and resolution factor of $I = 1$. Similarly, Fig. 8(c) and (d) illustrates the average MSE and BER, respectively, using PI with $N_p = 80$ and $I = 2$. With $N_p = 80$ and $I = 1$, the results match those of LS channel estimation seen in Fig. 6(a) and (b), where MSE saturation is observed at SNRs above 20 dB. This saturation is a consequence of the fact that the path delays of the equivalent downlink channel do not fall on the sampling grid, i.e., their delays are not multiples of T/K . The situation is remedied by using a resolution factor of $I = 2$, as seen in Fig. 8(c) and (d).

Fig. 9 depicts the results of a coherent system based on PI channel estimation for 8-PSK and 16-QAM modulation schemes. The PI channel estimation parameters used are $N_p = 80$ and $I = 2$.

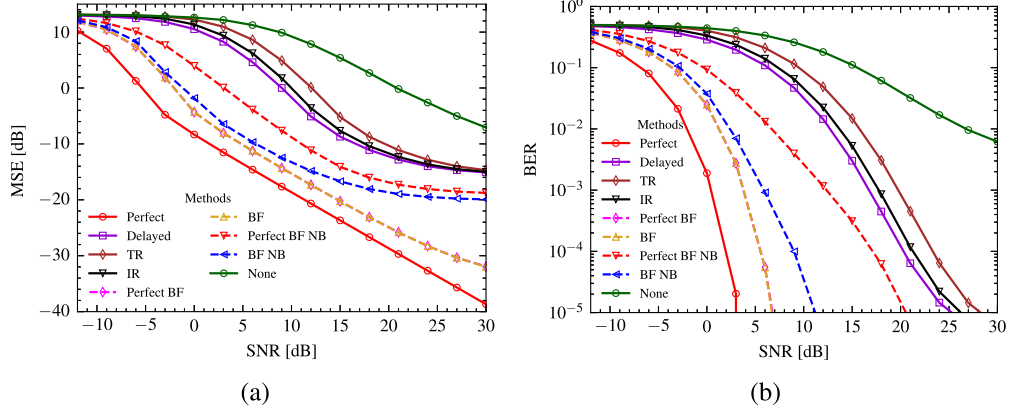


Fig. 6. Performance of various beamforming techniques: average data detection MSE (a) and BER (b) as functions of the input SNR. Coherent QPSK detection based on LS channel estimation is used at the receiver with $L_{dn} = 80$ channel taps and $K_{pil} = 128$ pilot carriers.

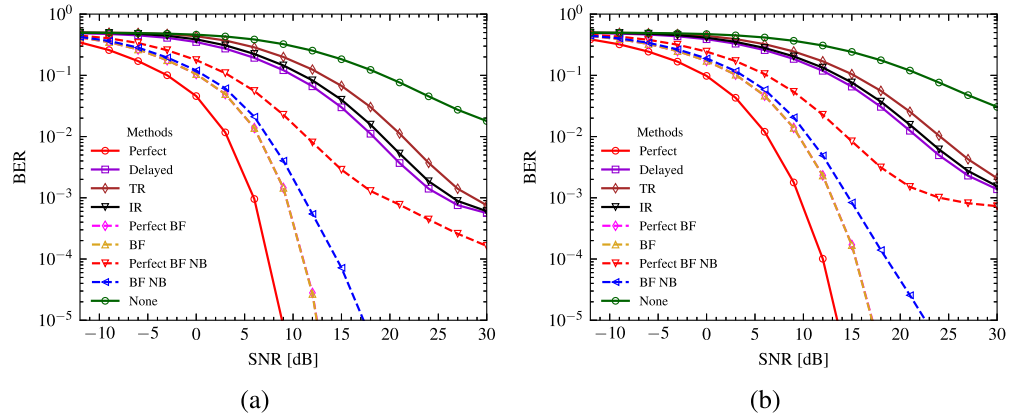


Fig. 7. Performance of various beamforming techniques in terms of BER as a function of the input SNR for (a) 8-PSK and (b) 16-QAM. Coherent detection based on LS channel estimation is used at the receiver with $L_{dn} = 80$ channel taps and $K_{pil} = 128$ pilot carriers.

In general, the coherent system performance trends match those of the differentially coherent detection, confirming that angle-based beamforming outperforms the channel-based techniques and is only surpassed by optimal beamforming.

In Fig. 10, we illustrate the power metric (8) and the relative path magnitudes $|h_p|$ positioned at true angles θ_p . In addition, the scatter plots of the detected data symbols for differentially coherent detection and coherent detection using LS and PI channel estimation are shown in Fig. 11(a)–(c), respectively. The channel estimation parameters are the ones used in Fig. 6(a) for LS and Fig. 8(c) for PI.

B. Beamforming With Null-Steering

Null-steering, described in Section III-D, allows the transmit array to set a beam in the direction of the principal path while simultaneously placing spatial nulls in the direction of other paths. We consider two null-steering strategies: broadband null-steering (NS), which requires computation of the beamforming vectors $\tilde{\mathbf{w}}_k$ for each carrier k , and narrowband null-steering (NS NB), that computes the beamforming vector $\tilde{\mathbf{w}}_0$ for the first carrier only and applies it to the carriers $k = 0, \dots, K - 1$. On the receiver side, either coherent detection or differentially coherent detection are implemented to estimate the data symbols.

To assess the performance of beamforming with null steering, we use a simulated underwater channel with the same parameters

as in Section IV-A. The channel exhibits $P = 5$ propagation paths, whose angles are estimated on the uplink using (8). The transmit array steers a beam in the principal path's direction and places spatial nulls in the direction of two next-strongest paths. The remaining two paths have lower energy [see Fig. 10(b)] and are not taken into account as they cannot be resolved by (8).

The downlink channel \mathbf{H}_k^{dn} experiences multipath that is covered by $L_{dn} = \lceil BT_{mp} \rceil$ impulse response taps spaced by T/K . However, when the transmitter employs null-steering to place spatial nulls in the directions of the paths other than the principal one, the channel is effectively shortened. The required number of channel taps needed to estimate the equivalent downlink channel coefficients \mathbf{H}_k^{eq} is $L_{eq} < L_{dn}$, if LS is being used. Similarly, the number of channel paths N_p and the total expected delay spread fed to the PI algorithm can also be shortened, thus reducing the overall complexity of the receiver.

Fig. 12 illustrates the comparison between the null-steering methods and the angle-based beamformers of Section IV-A, namely, broadband beamforming (case 6) and narrowband beamforming (case 8), for different values of input SNRs, 15 and 24 dB, and a varying number of channel equivalent taps L_{eq} and number of paths, which are fed to the LS and PI channel estimators, respectively.

Fig. 12(a) reveals that both narrowband beamforming and narrowband null-steering performances improve as the number of discrete taps L_{dn} increases. On the contrary, broadband

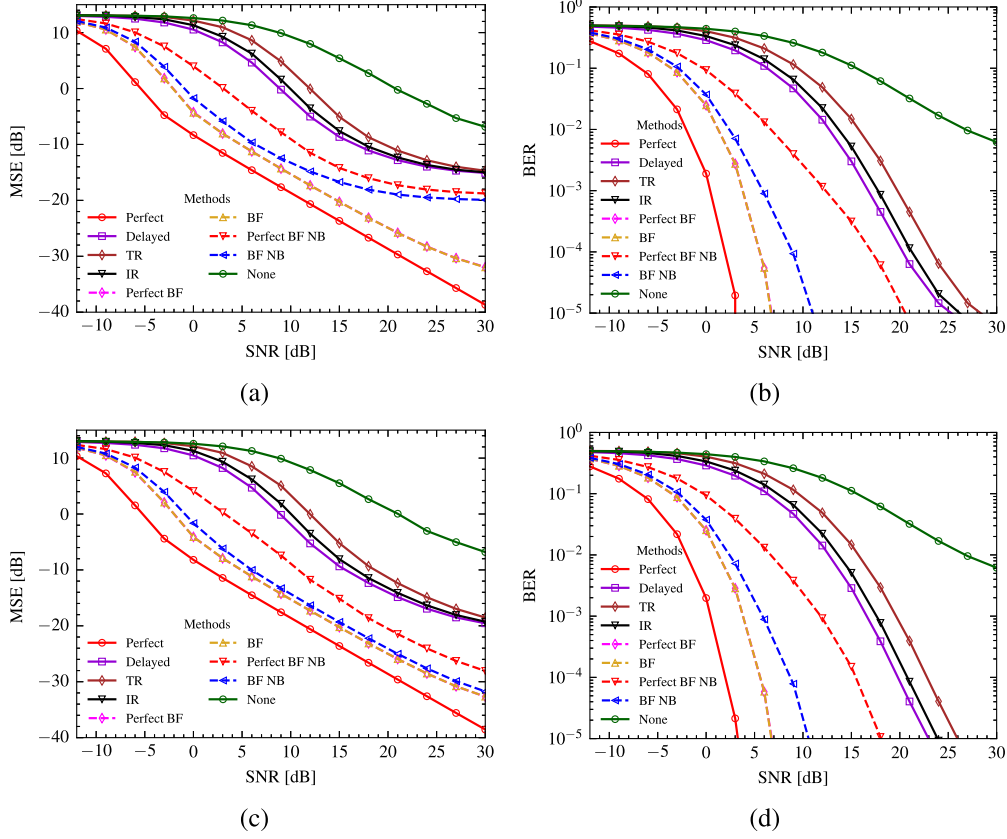


Fig. 8. Performance of various beamforming techniques: average data detection MSE (left column) and BER (right column) as functions of the input SNR. Coherent QPSK detection based on PI channel estimation is used at the receiver. The number of paths and resolution factor used by the PI algorithm are $N_p = 80$ and $I = 1$ in (a) and (b), and $N_p = 80$ and $I = 2$ in (c) and (d), with $K_{pil} = 128$ pilot carriers.

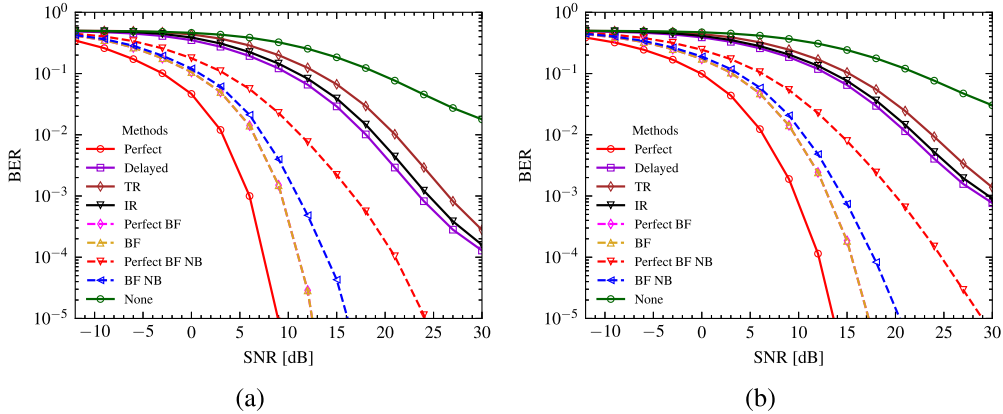


Fig. 9. Performance of various beamforming techniques in terms of BER as a function of the input SNR for 8-PSK (a) and 16-QAM (b). PI channel estimation is used at the receiver with $N_p = 80$, $I = 2$, and $K_{pil} = 128$ pilot carriers.

beamforming and broadband null-steering techniques remain insensitive to increasing the length of the channel estimator beyond the necessary minimum. Broadband null-steering method delivers extra 3–4 dB compared to the broadband beamforming approach.

Fig. 12(b) depicts the performance of various beamforming methods as a function of the number of channel paths N_p fed to the PI channel estimator. Similarly, broadband null-steering outperforms all the other angle-based beamforming techniques. We

observe in Fig. 12(b) that the performance of narrowband beamforming methods improves as more paths are taken into account, while the performance of the broadband beamforming techniques remains constant for the same range of number of paths.

Broadband beamforming techniques deliver a comparable performance for coherent detection based on LS and PI channel estimation. More notably, broadband null-steering surpasses other beamforming methods when only a few taps are used, e.g., $L_{eq} = 2$ for LS and a single path for PI receive-side

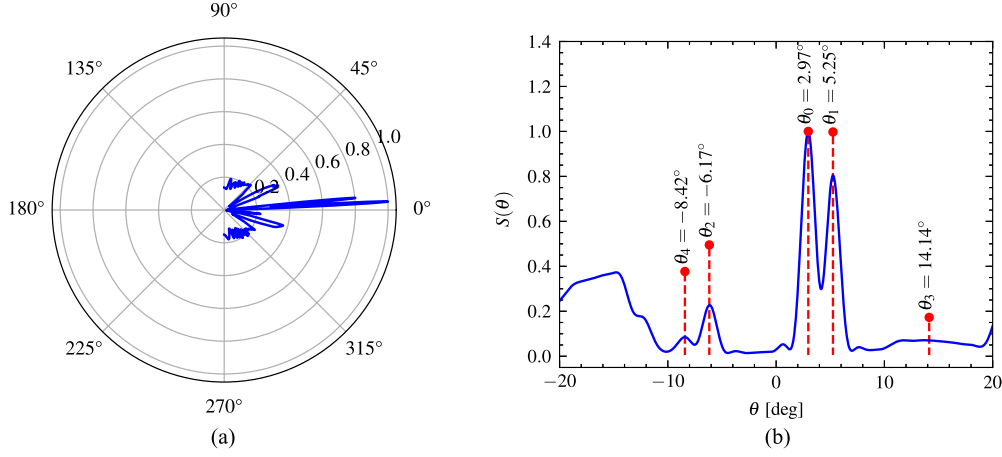


Fig. 10. (a) Power metric $S(\theta)$ used to estimate the principal path's angle of arrival θ_0 according to (8) and (9). The input SNR is 20 dB. The peak of $S(\theta)$ points in the direction of the principal path. (b) Red circles show the relative path magnitudes $|h_p|$ positioned at true angles θ_p .

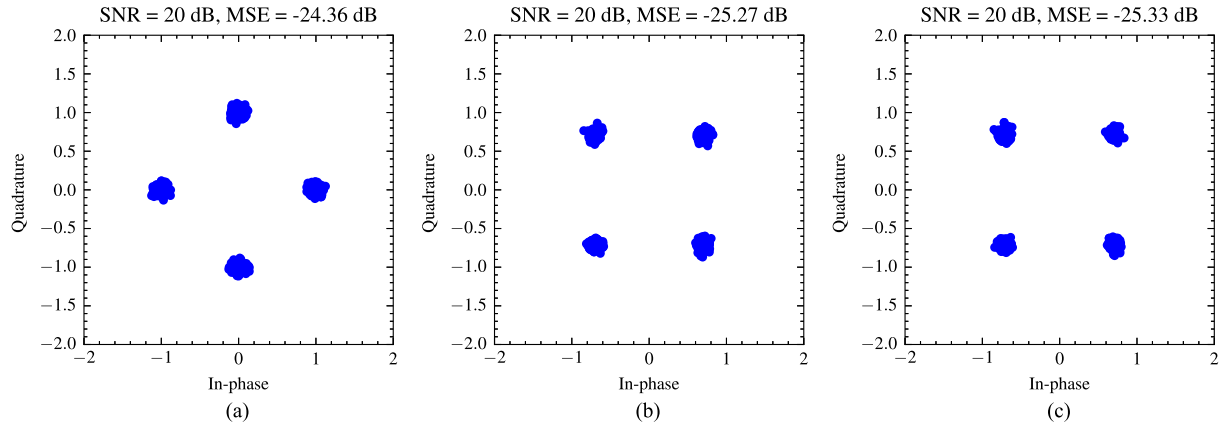


Fig. 11. Scatter plot of the estimated data symbols using (a) differentially coherent detection, (b) coherent detection with LS channel estimation, and (c) coherent detection with PI channel estimation. Beamforming is applied in the principal path's direction with the angle estimated from the power metric depicted in Fig. 10 (case 6 of Section IV-A). The input SNR is 20 dB.

channel estimation techniques, thus, allowing the use of a lower complexity receiver.

Fig. 13 shows the results of differentially coherent detection. Broadband null-steering performs comparably to broadband beamforming for the range of input SNRs shown and the performance trends are similar to those of coherent detection.

V. OPTIMAL ARRAY SELECTION

The results presented so far demonstrate the potential of transmit beamforming. This potential is contingent upon a proper design of the array, i.e., optimal selection of the interelement spacing and array aperture size. While multiple-input multiple-output (MIMO) systems that target spatial diversity on fading channels require the array elements to be sufficiently separated so that the observed signals are uncorrelated [19], conventional array processing theory suggests that array elements should be separated by less than one half of the shortest wavelength of the received signal [20]. Underwater acoustic channels, in addition to being broadband, exhibit particular geometry features that warrant revisiting of the optimal array design. In particular, the multipath signals may arrive from a limited range of angles.

In such a situation, the channel appears sparse in the vertical wave number domain [21], thus, alleviating the classical element spacing constraints. In this section, we address the issue of choosing the array geometry within the framework of transmit beamforming and broadband acoustic communications.

A. Element Spacing and Angular Resolution

The ability to resolve the multipath angles of arrival plays an important role when beamforming is performed in the direction of the principal path. The angular resolution mainly depends on the number of array elements and the interelement spacing. Assuming plane wave propagation, the angular resolution required to differentiate between two angles of arrival θ_p and θ_q is expressed as

$$2\pi f_k \frac{d}{c} (\sin \theta_p - \sin \theta_q) > \frac{2\pi}{M_t}, \quad k = 0, \dots, K-1. \quad (16)$$

In this inequality, the wavelength across the carriers is given by $\lambda_k = c/f_k$. Since $\lambda_k \in [\lambda_{\min}, \lambda_{\max}]$, we need $|\sin \theta_p - \sin \theta_q| > \lambda_{\max}/(M_t d)$ to satisfy (16). Thus, both the number of array elements M_t and the interelement spacing d

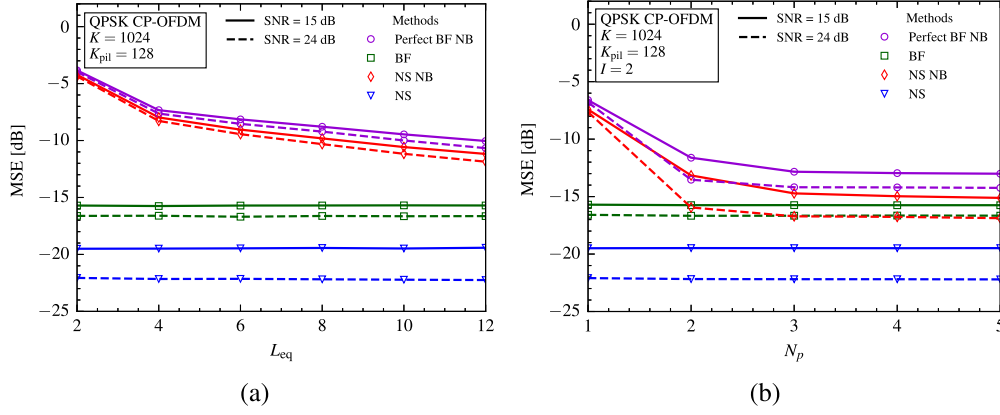


Fig. 12. Performance of various angle-based beamforming techniques using coherent QPSK detection. The plots illustrate the average MSE in data detection versus the number of channel taps L_{eq} (a) and the number of paths N_p (b) for channel estimation based on LS and PI algorithms, respectively.

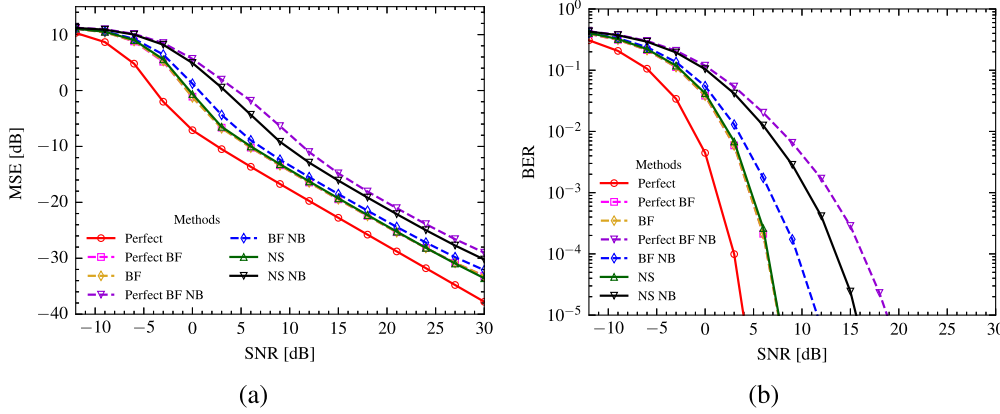


Fig. 13. Performance of various angle-based beamforming techniques, namely narrowband beamforming, broadband beamforming, narrowband null-steering, and broadband null-steering, using differentially coherent QPSK detection. The plots illustrate the average data detection MSE (a) and BER (b) as functions of the input SNR.

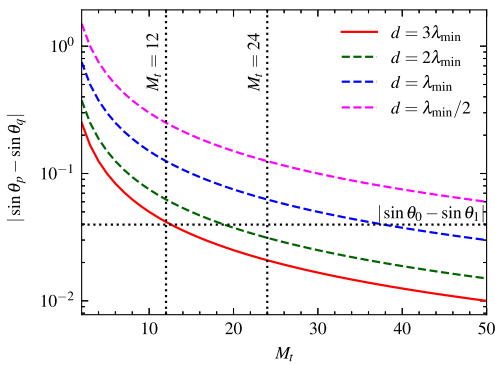


Fig. 14. Angular resolution bound $\lambda_{\min}/(M_t d)$, as a function of the number of array elements M_t for several choices of the interelement spacing d . The horizontal dotted line represents $|\sin \theta_0 - \sin \theta_1|$, the angles of two strongest arrivals of Fig. 10(b) ($\theta_0 = 2.9^\circ$ and $\theta_1 = 5.2^\circ$). If $d = 3\lambda_{\min}$, the angular resolution constraint (16) implies that these two paths will be resolvable if $M_t \geq 12$. If $d = 2\lambda_{\min}$, $M_t \geq 18$ or more elements are needed.

can be selected to achieve the desired angular resolution. Fig. 14 shows that arrays with smaller element spacing require a greater number of elements to achieve the same angular resolution as a system with larger interelement spacing.

The difference between the two spacing choices lies in the angular ambiguities they introduce. An array with a fixed number of elements and a larger interelement spacing improves the resolution, but introduces more ambiguities.

The angular ambiguity constraint for two signals impinging upon the array at angles θ_p and θ_q can be expressed as

$$2\pi f_k \frac{d}{c} (\sin \theta_p - \sin \theta_q) \leq 2\pi, \quad k = 0, \dots, K-1. \quad (17)$$

This condition implies that $|\sin \theta_p - \sin \theta_q| \leq \lambda_{\min}/d$.

It is worth noting at this point that in many practical applications one does not expect the signal to arrive from the full $\pm 90^\circ$ range, but from some smaller range $\pm \vartheta_{\max}$. If that is the case, the ambiguity condition can be appropriately adjusted. The two conditions are now combined into the final constraint

$$\frac{\lambda_{\max}}{M_t \Delta_{\min}} < d \leq \frac{\lambda_{\min}}{\Delta_{\max}} \quad (18)$$

where $\Delta_{p,q} = |\sin \theta_p - \sin \theta_q|$, and the paths (p, q) that should be considered in determining $\Delta_{\max} = \max_{p,q} \Delta_{p,q}$ and $\Delta_{\min} = \min_{p,q} \Delta_{p,q}$ include only the significant stable paths. The paths that are not significant do not contribute enough energy

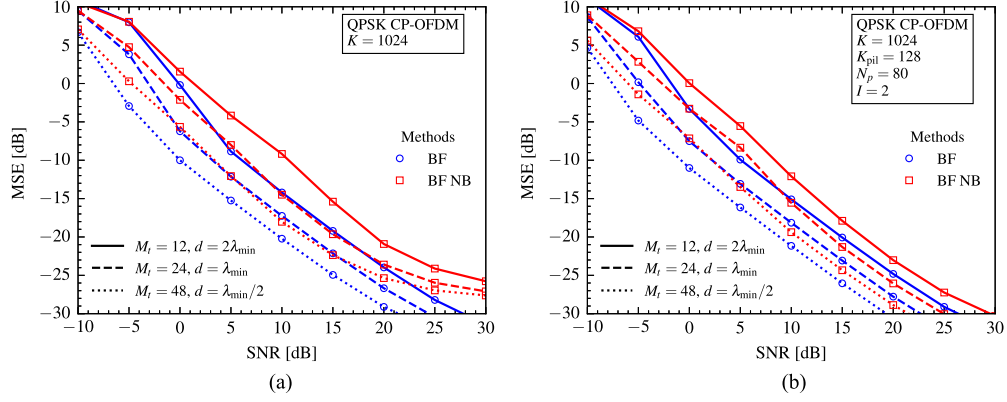


Fig. 15. Performance of angle-based beamforming techniques in terms of data detection MSE for varied number of transmit array elements M_t and interelement spacing d , for (a) differentially coherent detection and (b) coherent detection based on PI channel estimation.

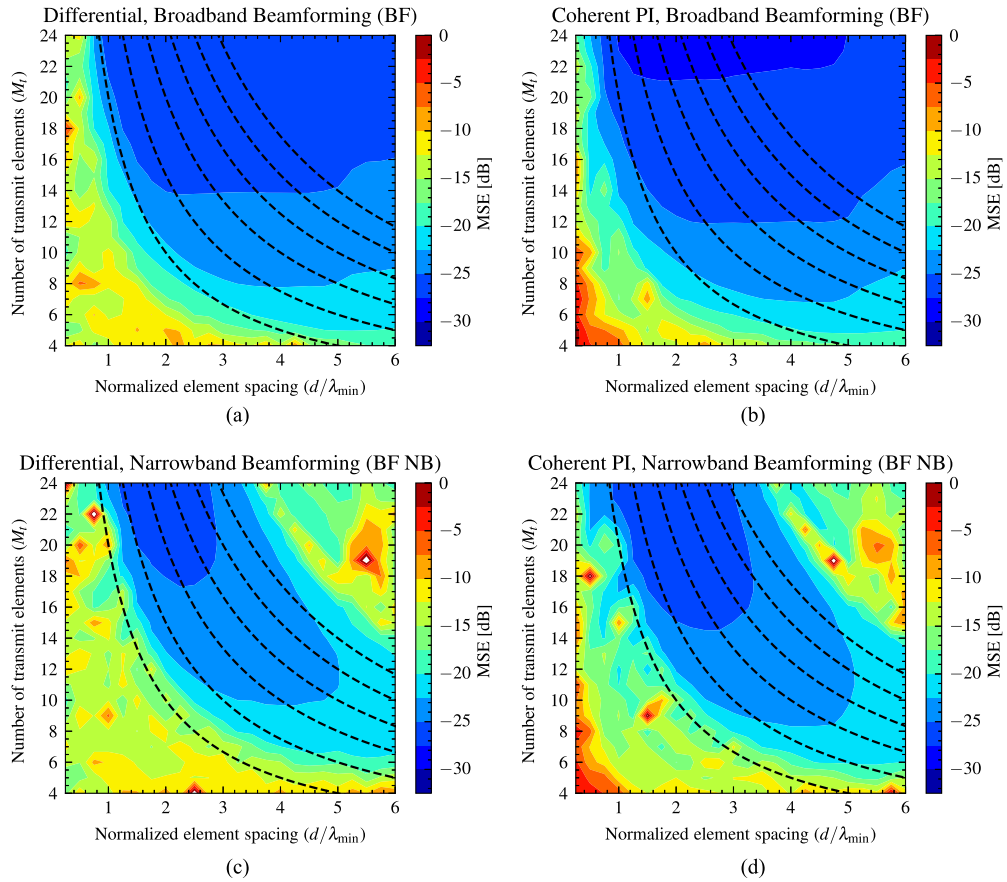


Fig. 16. Mean-squared error of the estimated data symbols for differentially coherent detection (a and c) and coherent detection (b and d) versus the number of transmitter elements M_t and interelement spacing d , in the context of broadband beamforming (a and b) and narrowband beamforming (c and d). The dashed lines represent the curves constant array aperture. The input SNR is 20 dB.

and can be neglected, while the paths that are not stable add incoherently and play no role in the design.

B. Impact of the Array Geometry on Angle-Based Beamforming Performance

We study the impact of the array geometry on the performance of angle-based beamforming techniques using synthetic data

transmitted through the shallow water channel whose parameters are given in Section IV. Specifically, we consider a varying number of array elements M_t and interelement spacings d normalized by the wavelength $\lambda_{\min} = c/f_{\max}$.

Performance of angle-based beamforming techniques for various array geometries is illustrated in Fig. 15. The number of elements is varied, but the aperture size, $M_t d$, is kept constant. We note that the use of more array elements reduces the MSE by

$10 \log_{10} M_t$, but more importantly, Fig. 15 reveals that if angular resolution is maintained, the system enables excellent detection performance for element spacing greater than $\lambda_{\min}/2$, which allows the use of fewer elements. As expected, coherent detection using PI algorithm [see Fig. 15(b)] outperforms the differentially coherent detection [see Fig. 15(a)] by approximately 3 dB.

Fig. 16 illustrates the MSE (color bar) versus the number of array elements M_t and interelement spacing d for a fixed SNR. For instance, the dark blue region indicates MSE below -25 dB. Therefore, any pair (M_t, d) that lies in the dark blue region will deliver a data detection MSE below -25 dB. Maintaining the data detection MSE at some specific level requires a tradeoff between the element spacing and the number of array elements. As shown in Fig. 16, the element spacing required for a certain MSE level decreases as the number of array elements increases, in such a way that the array aperture is approximately constant (note the lines of constant aperture) [21].

VI. TRACKING

For mobile acoustic systems, the principal path's angle can evolve over time, and the computation of (9) for each OFDM block of a frame might be intensive. Angular tracking is advantageous in such situations as it reduces the computation complexity and enables accurate broadband beamforming in a time-varying channel.

The tracking algorithm is based on the stochastic gradient descent. The gradient of $S(\theta)$ given in (8) is expressed as

$$\dot{S}(\theta) = \frac{\partial S(\theta)}{\partial \theta} = 2\text{Re} \left\{ \sum_{k=0}^{K-1} \dot{\mathbf{w}}_k^{\mathcal{H}}(\theta) \mathbf{x}_k^{\text{up}} (\mathbf{x}_k^{\text{up}})^{\mathcal{H}} \mathbf{w}_k(\theta) \right\} \quad (19)$$

where the gradient of $\mathbf{w}_k(\theta)$ with respect to θ is

$$\dot{\mathbf{w}}_k(\theta) = \begin{bmatrix} \dot{w}_k^0(\theta) & \dot{w}_k^1(\theta) & \dots & \dot{w}_k^{M_t-1}(\theta) \end{bmatrix}^{\top}.$$

The partial derivative $\partial w_k^m(\theta)/\partial \theta$ is given by $\dot{w}_k^m(\theta) = -jm\dot{\psi}_k(\theta)e^{-j\psi_k(\theta)}$ with $\psi_k(\theta) = 2\pi f_k(d/c) \sin \theta$ and $\dot{\psi}_k(\theta) = 2\pi f_k(d/c) \cos \theta$.

The update step at block n is formulated as

$$\hat{\theta}_0(n+1) = \hat{\theta}_0(n) + \mu_{\theta} \dot{S}(\hat{\theta}_0(n)) \quad (20)$$

where μ_{θ} is the step size. Assuming that the initial estimate is obtained from the first OFDM block of a frame, tracking evolves through the rest of the blocks. The blocks are indexed by $n = 0, 1, \dots, N_b - 1$, and the gradient at time n , $\dot{S}(\theta)$, is calculated using the corresponding values $\mathbf{x}_k^{\text{up}}(n)$ and $\theta = \hat{\theta}_0(n)$.

Angle estimation involves finding the maximum of the function (8), which does not have a single global maximum, but instead has several local maxima. Gradient descent thus has to be applied carefully, making sure that the search begins at a proper initial point and progresses in small steps. While this may sound non-intuitive, consideration of the system geometry reveals that the change in angle from one block to the next is indeed very small. For example, with the system of Section IV, motion of the receiver at 1 m/s will cause the angle to change only by 0.01° during one OFDM block. Hence, an accurate initial estimate

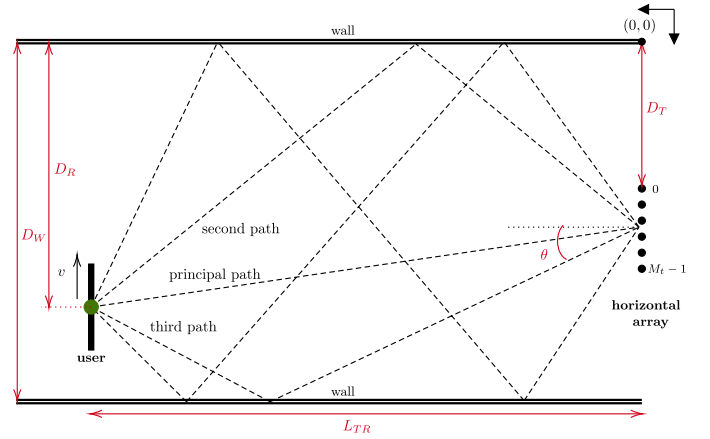


Fig. 17. System geometry of the over-the-air channel (top view).

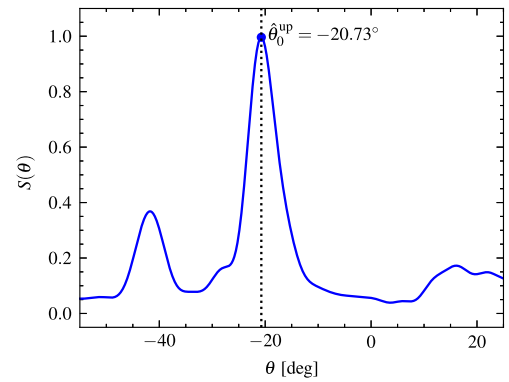


Fig. 18. Power metric $S(\theta)$ used to estimate the principal path's angle of arrival θ_0 in the uplink.

$\hat{\theta}_0(0)$ obtained from full-scale maximization and a well-chosen step-size are expected to keep the tracking loop stable.

VII. EXPERIMENTAL RESULTS

As a proof of concept, we tested the transmit beamforming techniques using experimental over-the-air transmissions in an indoor environment of the acoustic communications testbed (ACT) developed at Northeastern University [22]. The environment used in the experiment is a room whose geometry is illustrated in Fig. 17. The width of the room is $D_W = 3.5$ m and the distance between the transmitter and the receiver is $L_{TR} = 3$ m. The horizontal locations of the transmitter and receiver are $D_T = 2$ m and $D_R = 3$ m, respectively. The setup consists of a horizontal transceiver array composed of $M_t = 12$ elements with interelement spacing $d = 5$ cm and a receive-end single transceiver, operating in the 5–8 kHz acoustic band. We present experimental results of transmit beamforming strategies, specifically the time-reversal and impulse-response for the channel-based beamforming, broadband beamforming, and narrowband beamforming for the angle-based beamforming.

A. Experiment

The experiment was performed using a QPSK cyclic-prefix (CP) OFDM signal, with initial carrier frequency

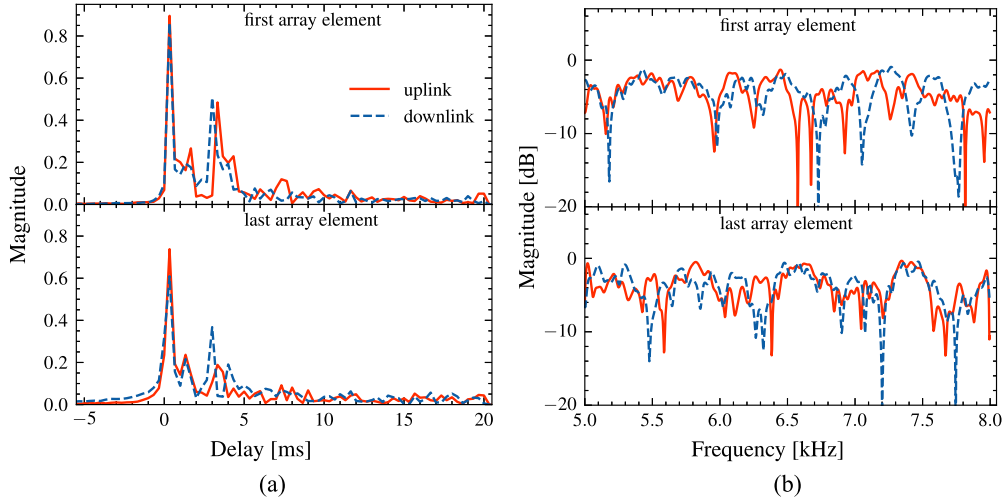


Fig. 19. Impulse responses (a) and transfer functions (b) of the channel measured on the uplink and downlink.

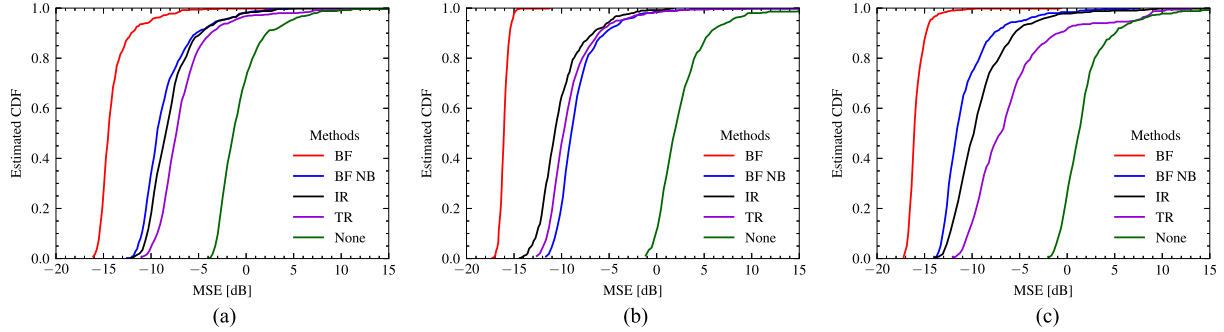


Fig. 20. Estimated CDF of the MSE in data detection for various transmit-side beamforming techniques. The CDFs reflect 500 uplink-downlink transmissions of a QPSK CP-OFDM system with $K = 1024$ carriers. The MSE is defined by (21) for differentially coherent detection and by (22) for coherent detection.

$f_0 = 5$ kHz, bandwidth $B = 3$ kHz, $K = 1024$, and guard interval $T_g = 32$ ms. Frequency offset compensation is applied to counteract the motion-induced Doppler shifts, according to the method introduced in [2].

The user moves in parallel with respect to the array (the direction in which the principal path's angle changes the most), at the speed $v = 0.2$ m/s. This speed may cause a Doppler shift of $(v/c)f_0 = 2.9$ Hz. In an underwater scenario, the same Doppler shift would be experienced by a vehicle moving at $v = 0.43$ m/s and $f_0 = 10$ kHz. After proper time synchronization, frequency offset compensation, and FFT demodulation, information symbols sent by the array are detected using differentially coherent detection as well as coherent detection based on LS and PI channel estimation.

The principal path's angle of arrival is estimated on the uplink by finding the peak of the metric $S(\theta)$ as in (9). The result is shown in Fig. 18. The estimated principal path's angle, $\hat{\theta}_0^{\text{up}} = -20.73^\circ$, is used to construct the beamforming weights $w_k^m(\hat{\theta}_0^{\text{up}})$ (7) that are implemented on the downlink (2).

For channel-based beamforming strategies, time-reversal and impulse response methods are implemented. The beamforming weights are constructed using the pilot signal (5) measured on the uplink. For the impulse response beamforming method, the uplink channel is estimated using $L_{\text{up}} = 80$ taps. In Fig. 19(a)

and (b), we illustrate the channel responses estimated on the uplink and downlink, respectively. The differences between uplink and downlink are notable.

The system performance is summarized in Fig. 20 which illustrates the estimated cumulative distribution function (CDF) of the MSE for 500 uplink-downlink transmissions. The MSE corresponding to an OFDM block with K carriers is measured in the i th transmission as

$$\text{MSE}(i) = \frac{1}{K-1} \sum_{k=1}^{K-1} |b_k^{\text{dn}}(i) - \hat{b}_k^{\text{dn}}(i)|^2 \quad (21)$$

and

$$\text{MSE}(i) = \frac{1}{K - K_{\text{pil}}} \sum_{k \notin \mathcal{K}_{\text{pil}}} |d_k^{\text{dn}}(i) - \hat{d}_k^{\text{dn}}(i)|^2 \quad (22)$$

for differentially coherent detection and coherent detection, respectively.

Evidently, beamforming in the principal path's direction outperforms the other transmit-side beamforming methods whether the receiver implements coherent or differentially coherent detection. Our experimental results, thus confirm that angle-based beamforming, albeit suboptimal when the channel is known perfectly at the transmitter, withstands the long feedback delay

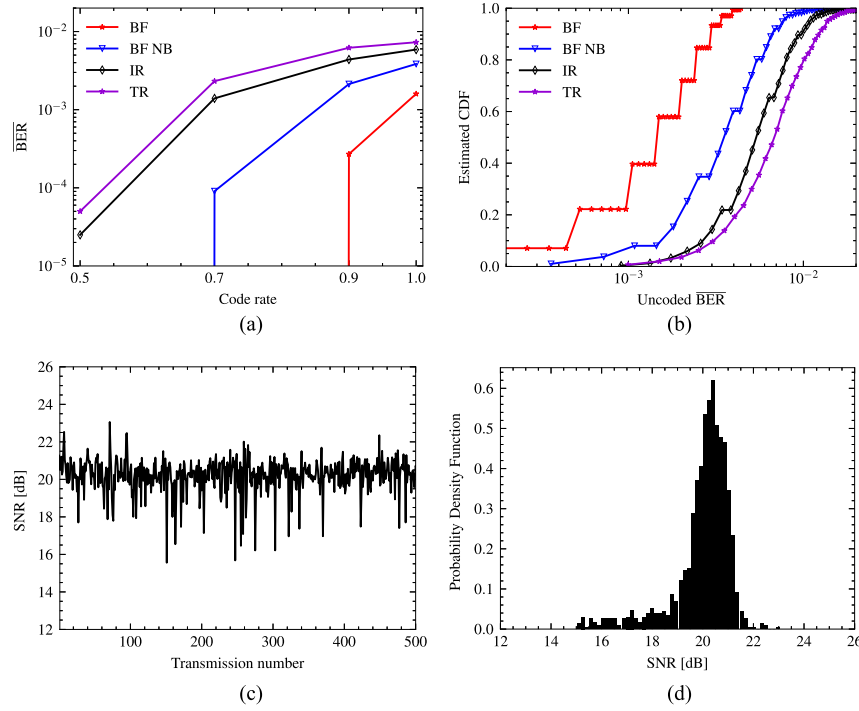


Fig. 21. Experimentally measured average BER of a QPSK CP-OFDM system with $K = 1024$. The transmitter utilizes various transmit-side beamforming methods and the receiver implements coherent detection with channel estimation based on PI. (a) Average BER as a function of the rate of the Polar code. (b) Estimated CDF of the uncoded average BER. (c) Instantaneous SNR computed for each of the 500 over-the-air transmissions. (d) Estimated PDF of the instantaneous SNR.

of the acoustic channel and delivers excellent performance in practical situations when the channel is only estimated.

In Fig. 21, we demonstrate the performance of several beamforming strategies in terms of the downlink average BER achieved using Polar codes for a range of code rates $\rho = 0.5, 0.7, 0.9$, and 1. Polar codes are known to achieve the capacity of the binary-input memoryless and the symmetric additive white Gaussian noise channels [23]. The codeword length is fixed to $N = 512$ and the number of codewords per OFDM block is $2K/N$ for QPSK, i.e., each OFDM block contains four codewords. With a code rate of 0.5, 256 data bits and a 16-b CRC are fed to the encoder; thus, the effective throughput is 4×240 information bits per OFDM block. We utilize a systematic encoder, whose channel reliability index is given in the [24, Table 5.3.1.2-1]. The receiver employs soft decision decoding, which uses the likelihood ratio of each received bit as an input, along with a list decoder to exploit the cyclic redundancy check (CRC) [25]. The encoder and decoder are implemented using the AFF3CT library [26]. A superior performance of the coded system is observed in Fig. 21(a) when the transmitter employs broadband beamforming (BF) in conjunction with coherent QPSK detection with channel estimation based on PI at the receiver. For a code rate of 0.9 and 1, BF achieves a BER of 2.7×10^{-4} and 1.6×10^{-3} , respectively. Code rates below 0.9 produce BER values that cannot be measured with the number of transmissions used in the experiment. BF NB delivers a BER of 9×10^{-5} , 2.1×10^{-3} , and 3.8×10^{-3} , for code rates of 0.7, 0.9, and 1, respectively. On the contrary, channel-based beamforming techniques show moderate performance results. IR and TR achieve a BER of 5.9×10^{-3} and 7.3×10^{-3} for a code rate of 1, respectively. For a code rate of 0.5, IR and TR achieve

an improved BER of 2.5×10^{-5} and 5×10^{-5} , respectively. Fig. 21(b) shows the estimated CDF of the uncoded average BER measured in the experiment. The SNR measured over the 500 transmissions is shown in Fig. 21(c) and its estimated probability density function (PDF) is illustrated in Fig. 21(d).

B. Tracking

The results of angle tracking are presented in Fig. 22. On the uplink, the user transmits an OFDM pilot signal with $N_b = 16$ blocks while it is moving in parallel with respect to the array at a relatively high speed of 0.2 m/s. The moving trajectory of the user equipment is illustrated in Fig. 17, and the step size of the gradient descent algorithm is $\mu_\theta = 25 \times 10^{-3}$. Fig. 22(b) reveals that the principal path's angle can be accurately tracked by stochastic gradient descent even when the receiver changes its direction, thus reducing the computation complexity on the transmit side. The duration of the OFDM block is $T = 0.2048$ s, and the angle is changing at a rate of approximately 0.7° per OFDM block.

VIII. CONCLUSION

We investigated transmit beamforming techniques suitable for underwater acoustic communications with long feedback delays. Conventional channel-based transmit beamforming requires complete channel knowledge at the transmit side; however, the time-varying nature of the acoustic channels, along with the long feedback delays, causes the transmitter to have only partial and outdated channel knowledge. To counteract this problem, we proposed an angle-based beamforming technique that targets transmission in the direction of a stable, principal

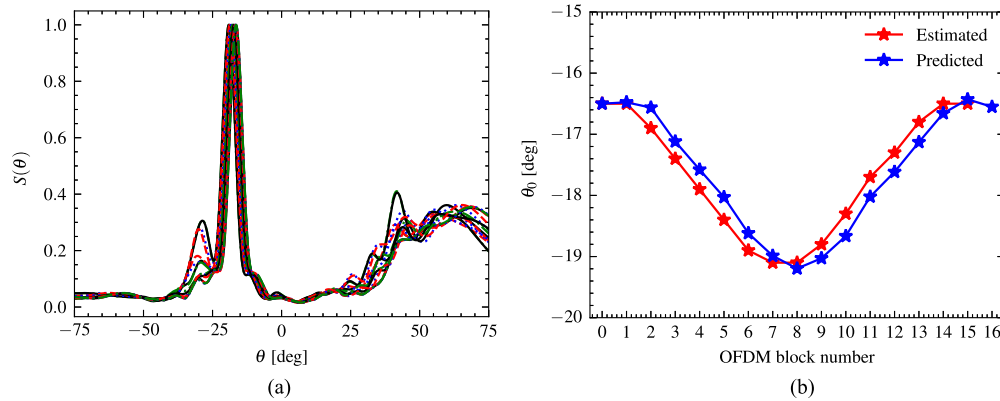


Fig. 22. (a) Evolution of the metric $S(\theta)$. (b) Angle tracking.

path only. While suboptimal as compared to the channel-based beamforming with perfect channel knowledge, this technique outperforms channel-based beamforming in a practical situation with an outdated and noisy channel estimate. The technique capitalizes on the fact that unlike the entire channel transfer function, which may change considerably over the time it takes to close the feedback loop, the angle of the principal stable path changes only negligibly.

We presented a comparative performance analysis using simulated data transmitted over a 1 km shallow water channel in the 10–15 kHz band. The angle-based beamforming using the estimated principal path's angle of arrival was shown to outperform channel-based beamforming, thus, emerging as a practical technique for transmit beamforming in acoustic communications. Its computational complexity is well within the limits of current processing power, requiring only a single angle estimate based on which the weights of a broadband beamformer are calculated.

We additionally demonstrated the potential of transmit beamforming strategies using over-the-air acoustic communications. The experimental results confirmed that angle-based beamforming is an effective transmit-side beamforming technique that surpasses channel-based beamforming methods.

In addition, we introduced an angle tracking method based on the stochastic gradient descent for mobile acoustic systems. Gradient descent significantly reduces the computational complexity, and maintains accurate broadband beamforming in a time-varying channel.

Future research will focus on investigating the possibilities of beamforming in directions of multiple stable paths, which is expected to yield further improvements in channels whose propagation conditions warrant the existence of such paths. In addition, current results encourage future research into transmit beamforming for multiple users in band-limited acoustic networks.

REFERENCES

- [1] Y. M. Aval and M. Stojanovic, "Differentially coherent multichannel detection of acoustic OFDM signals," *IEEE J. Ocean. Eng.*, vol. 40, no. 2, pp. 251–268, Apr. 2015.
- [2] A. Tadayon and M. Stojanovic, "Low-complexity superresolution frequency offset estimation for high data rate acoustic OFDM systems," *IEEE J. Ocean. Eng.*, vol. 44, no. 4, pp. 932–942, Oct. 2019.
- [3] A. Tadayon and M. Stojanovic, "Iterative sparse channel estimation and spatial correlation learning for multichannel acoustic OFDM systems," *IEEE J. Ocean. Eng.*, vol. 44, no. 4, pp. 820–836, Oct. 2019.
- [4] E. Björnson, M. Bengtsson, and B. Ottersten, "Optimal multiuser transmit beamforming: A difficult problem with a simple solution structure [lecture notes]," *IEEE Signal Process. Mag.*, vol. 31, no. 4, pp. 142–148, Jul. 2014.
- [5] A. Song, M. Stojanovic, and M. Chitre, "Editorial underwater acoustic communications: Where we stand and what is next?," *IEEE J. Ocean. Eng.*, vol. 44, no. 1, pp. 1–6, Jan. 2019.
- [6] A. Radosevic, R. Ahmed, T. M. Duman, J. G. Proakis, and M. Stojanovic, "Adaptive OFDM modulation for underwater acoustic communications: Design considerations and experimental results," *IEEE J. Ocean. Eng.*, vol. 39, no. 2, pp. 357–370, Apr. 2014.
- [7] W. A. Kuperman, W. S. Hodgkiss, H. C. Song, T. Akal, C. Ferla, and D. R. Jackson, "Phase conjugation in the ocean: Experimental demonstration of an acoustic time-reversal mirror," *J. Acoustical Soc. Amer.*, vol. 103, no. 1, pp. 25–40, 1998.
- [8] G. Edelmann, H. Song, S. Kim, W. Hodgkiss, W. Kuperman, and T. Akal, "Underwater acoustic communications using time reversal," *IEEE J. Ocean. Eng.*, vol. 30, no. 4, pp. 852–864, Oct. 2005.
- [9] M. Stojanovic, "Retrofocusing techniques for high rate acoustic communications," *J. Acoustical Soc. Amer.*, vol. 117, no. 3, pp. 1173–1185, Mar. 2005.
- [10] L. Liao, Y. V. Zakharov, and P. D. Mitchell, "Underwater localization based on grid computation and its application to transmit beamforming in multiuser UWA communications," *IEEE Access*, vol. 6, pp. 4297–4307, 2018.
- [11] M. Rahmati and D. Pompili, "SSFB: Signal-space-frequency beamforming for underwater acoustic video transmission," in *Proc. IEEE 14th Int. Conf. Mobile Ad Hoc Sensor Syst.*, 2017, pp. 180–188.
- [12] M. Rahmati and D. Pompili, "Probabilistic spatially-divided multiple access in underwater acoustic sparse networks," *IEEE Trans. Mobile Comput.*, vol. 19, no. 2, pp. 405–418, Feb. 2020.
- [13] J. Capon, "High-resolution frequency-wavenumber spectrum analysis," *Proc. IEEE*, vol. 57, no. 8, pp. 1408–1418, Aug. 1969.
- [14] P. Stoica and A. Nehorai, "MUSIC, maximum likelihood and Cramer-Rao bound: Further results and comparisons," in *Proc. Int. Conf. Acoust. Speech Signal Process.*, 1989, pp. 2605–2608.
- [15] R. Roy and T. Kailath, "ESPRIT-Estimation of signal parameters via rotational invariance techniques," *IEEE Trans. Acoust. Speech Signal Process.*, vol. 37, no. 7, pp. 984–995, Jul. 1989.
- [16] P. Qarabaqi and M. Stojanovic, "Statistical characterization and computationally efficient modeling of a class of underwater acoustic communication channels," *IEEE J. Ocean. Eng.*, vol. 38, no. 4, pp. 701–717, Apr. 2013.
- [17] T. K. Lo, "Maximum ratio transmission," *IEEE Trans. Commun.*, vol. 47, no. 10, pp. 1458–1461, Oct. 1999.
- [18] B. Friedlander and B. Porat, "Performance analysis of a null-steering algorithm based on direction-of-arrival estimation," *IEEE Trans. Acoust., Speech, Signal Process.*, vol. 37, no. 4, pp. 461–466, Apr. 1989.

- [19] D. Gesbert, M. Shafi, D. Shiu, P. J. Smith, and A. Naguib, "From theory to practice: An overview of MIMO space-time coded wireless systems," *IEEE J. Sel. Areas Commun.*, vol. 21, no. 3, pp. 281–302, Apr. 2003.
- [20] H. L. V. Trees, *Optimum Array Processing*. Hoboken, NJ, USA: Wiley, 2002.
- [21] M. Pajovic and J. C. Preisig, "Performance analysis and optimal design of multichannel equalizer for underwater acoustic communications," *IEEE J. Ocean. Eng.*, vol. 40, no. 4, pp. 759–774, Oct. 2015.
- [22] D. A. Cuji, Z. Li, and M. Stojanovic, "ACT: An acoustic communications testbed," in *Proc. IEEE Conf. Comput. Commun. Workshops*, 2022, pp. 1–6.
- [23] E. Arikan, "Channel polarization: A method for constructing capacity-achieving codes for symmetric binary-input memoryless channels," *IEEE Trans. Inf. Theory*, vol. 55, no. 7, pp. 3051–3073, Jul. 2009.
- [24] 3GPP TS 38.212 v15.2.0, "Technical Specification 5G; NR; Multiplexing and channel coding," Jun. 2018.
- [25] I. Tal and A. Vardy, "List decoding of polar codes," *IEEE Trans. Inf. Theory*, vol. 61, no. 5, pp. 2213–2226, May 2015.
- [26] A. Cassagne et al., *AFF3CT: A Fast Forward Error Correction Toolbox!*, vol. 10. Amsterdam, The Netherlands: Elsevier, 2019, Art. no. 100345.



Diego A. Cuji (Graduate Student Member, IEEE) received the B.S. degree in electronic engineering from Universidad Politecnica Salesiana, Cuenca, Ecuador, in 2014 and the M.S. degree in electrical and computer engineering in 2019 from Northeastern University, Boston, MA, USA, where he is currently working toward the Ph.D. degree in electrical engineering.

His research interests include digital communications, OFDM, beamforming, and underwater acoustic communications.



Milica Stojanovic (Fellow, IEEE) received the graduation degree in electrical engineering from the University of Belgrade, Belgrade, Serbia, in 1988, and the M.S. and Ph.D. degrees in electrical engineering from Northeastern University, Boston, MA, USA, in 1991 and 1993, respectively.

She was a Principal Scientist at MIT, and in 2008 joined Northeastern University, Boston, MA, USA, where she is currently a Professor of Electrical and Computer Engineering. She is also a Guest Investigator with the Woods Hole Oceanographic Institution,

Woods Hole, MA, USA. Her research interests include digital communications theory, statistical signal processing and wireless networks, and their applications to underwater acoustic systems.

Dr. Stojanovic is an Associate Editor for *IEEE Journal of Oceanic Engineering*, and a past Associate Editor for *IEEE TRANSACTIONS ON SIGNAL PROCESSING* and *IEEE TRANSACTIONS ON VEHICULAR TECHNOLOGY*. She chairs the IEEE Ocean Engineering Society (OES) Technical Committee for Underwater Communication, Navigation and Positioning, and serves on the Editorial Board of *IEEE Signal Processing Magazine*. She is the recipient of the 2015 IEEE/OES Distinguished Technical Achievement Award, and the 2018 IEEE/OES Distinguished Lecturer. In 2022, she was awarded an honorary doctorate from the Aarhus University in Denmark, and she was elected into the Academy of Engineering Sciences of Serbia.